AD NUMBER
AD014592
CLASSIFICATION CHANGES
TO: **UNCLASSIFIED**
FROM: **CONFIDENTIAL**
LIMITATION CHANGES
TO: **Approved for public release; distribution is unlimited.**
FROM: **Distribution authorized to U.S. Gov't. agencies and their contractors; Administrative/Operational Use; 17 SEP 1952. Other requests shall be referred to National Aeronautics and Space Administration, Washington, DC.**
AUTHORITY
NASA memo dtd 18 Feb 1963 NASA TR Server website

SECURITY INFORMATION

[redacted]

c.1

Copy 43
RM SL52I12

NACA

RESEARCH MEMORANDUM

for the

U. S. Air Force

FLIGHT DETERMINATION OF THE LONGITUDINAL

STABILITY OF A $\frac{1}{10}$-SCALE ROCKET-POWERED MODEL OF THE

NORTHROP MX-775A MISSILE AT LOW LIFT COEFFICIENTS

AND MACH NUMBERS FROM 0.89 TO 1.34

By Warren Gillespie, Jr., and Richard G. Arbic

Langley Aeronautical Laboratory
Langley Field, Va.

[redacted]

NATIONAL ADVISORY COMMITTEE FOR AERONAUTICS

WASHINGTON

SEP 17 1952

[redacted]

NACA RM SL52I12

NATIONAL ADVISORY COMMITTEE FOR AERONAUTICS

RESEARCH MEMORANDUM

for the

U. S. Air Force

FLIGHT DETERMINATION OF THE LONGITUDINAL STABILITY OF A $\frac{1}{10}$-SCALE ROCKET-POWERED MODEL OF THE NORTHROP MX-775A MISSILE AT LOW LIFT COEFFICIENTS AND MACH NUMBERS FROM 0.89 TO 1.34

By Warren Gillespie, Jr., and Richard G. Arbic

SUMMARY

A flight investigation has been made to determine the longitudinal stability of a $\frac{1}{10}$-scale model of the Northrop MX-775A missile at low lift coefficients through a range of Mach number from 0.89 to 1.34. The model was disturbed in pitch by small pulse rockets. The pitching response of the model was analyzed to obtain the longitudinal stability characteristics. Some information relating to the directional stability characteristics was also obtained. The data are compared with wind-tunnel measurements from a $\frac{1}{15}$-scale model at high subsonic and supersonic Mach numbers reported in NACA RM A51E28.

Aeroelastic deflections of the 75S-T6 solid-aluminum-alloy wing of the present test model reduced the lift-curve slope approximately 25 percent from rigid wing values and shifted the model aerodynamic center forward by approximately 15 percent of the mean aerodynamic chord. The lift-curve slope had a maximum value of approximately 0.070 at a Mach number of 1. At this same Mach number, the lift-curve slope corrected for the effect of aeroelastic deflection was 0.095. The aerodynamic center moved from the most forward location of 10-percent mean aerodynamic chord at a Mach number of 0.9 to the most rearward location of 20-percent mean aerodynamic chord at a Mach number of 1.2. The aerodynamic center corrected for aeroelastic effect moved from

22-percent mean aerodynamic chord at a Mach number of 0.9 to the most rearward location of 39 percent at a Mach number of 1.34. The static stability increased as the Mach number became supersonic. The rotational damping $(C_m)_{\dot{\theta}\bar{c}/2V} + (C_m)_{\dot{\alpha}\bar{c}/2V}$ became relatively low at transonic Mach numbers and was at a minimum near Mach number 1; however, the total damping increased as the Mach number became supersonic.

INTRODUCTION

An investigation of the longitudinal stability of $\frac{1}{10}$-scale rocket-powered models of the Northrop MX-775A missile from high subsonic to low supersonic speeds is being conducted by the Langley Pilotless Aircraft Research Division at the request of the U. S. Air Force.

The Northrop missile is a jet-propelled, long-range, ground-to-ground missile designed to cruise at high subsonic speeds and to attain supersonic Mach numbers during the terminal approach to the target. The missile has a highly swept, thin wing with a large aspect ratio. Aeroelastic deflections encountered with such a wing may cause large variations in the stability of the missile. The over-all investigation considers the effects of different model wing stiffness on the longitudinal characteristics.

The primary purpose of this test is to determine the longitudinal stability at low lift coefficients of a $\frac{1}{10}$-scale model having a solid wing of 75S-T6 solid aluminum alloy and to estimate the static stability of the missile configuration for the case of a rigid wing.

SYMBOLS

a	acceleration, ft/sec^2
A	wing aspect ratio, b^2/S
b	wing span, ft
c	local wing chord
$\bar{c}$	wing mean aerodynamic chord, ft
c_{ave}	average wing chord, ft

C_C chord-force coefficient, positive in a forward direction, $\frac{a_l}{g}\frac{W}{S}\frac{l}{q}$

C_D drag coefficient, $C_N \sin \alpha - C_C \cos \alpha$

C_L lift coefficient, $C_N \cos \alpha + C_C \sin \alpha$

C_l section lift coefficient

C_m pitching-moment coefficient, $\frac{\text{Pitching moment about center of gravity}}{qS\bar{c}}$

C_n yawing-moment coefficient, $\frac{\text{Yawing moment about center of gravity}}{qSb}$

C_N normal-force coefficient, positive toward top of model from model center line, $\frac{a_n}{g}\frac{W}{S}\frac{l}{q}$

$\frac{C_l c}{C_L c_{ave}}$ span-load coefficient

g acceleration due to gravity, 32.2 ft/sec^2

I_y moment of inertia about pitch axis

I_z moment of inertia about directional axis

K aeroelastic correction factor

L measured lift

M Mach number

P period, sec

q dynamic pressure, $\rho V^2/2$, lb/sq ft

R Reynolds number based on wing mean aerodynamic chord

S wing area including body intercept

$T_{1/2}$ time to damp to one-half amplitude, sec

V	velocity, ft/sec
W	weight of model, lb
y	spanwise station, ft
$\bar{y}$	spanwise center of pressure (rigid wing), ft
$\bar{y}_{\Delta L}$	spanwise center of pressure of ΔL, ft
$\Lambda_{c/4}$	sweep angle of quarter-chord line, deg
α	angle of attack at model center of gravity, deg
ρ	air density, slugs/cu ft
Δ	increment
θ	angle between fuselage center line and horizontal, radians
γ	change in flight-path angle, radians

$\dot{\theta} = \frac{d\theta}{dt}$, radians/sec

$\ddot{\theta} = \frac{d^2\theta}{dt^2}$, radians/sec^2

$\dot{\alpha} = \frac{d\alpha}{dt}$, radians/sec

$\dot{\gamma} = \frac{d\gamma}{dt}$, radians/sec

The derivatives are expressed as follows:

$$C_{L_\alpha} = \frac{\partial C_L}{\partial \alpha} \qquad C_{n_\beta} = \frac{\partial C_n}{\partial \beta} \qquad C_{m_\alpha} = \frac{\partial C_m}{\partial \alpha}$$

$$(C_m)_{\dot{\theta}\bar{c}/2V} = \frac{\partial C_m}{\partial \frac{\dot{\theta}\bar{c}}{2V}} \qquad (C_m)_{\dot{\alpha}\bar{c}/2V} = \frac{\partial C_m}{\partial \frac{\dot{\alpha}\bar{c}}{2V}}$$

MODEL

A three-view drawing of the $\frac{1}{10}$-scale model used in the present investigation is shown in figure 1. Photographs of the model are shown in figures 2 and 3. Table I gives the dimensional and mass characteristics and table II gives the model ordinates. The model was similar to the winged model of reference 1. For this test, the nose of the model was lengthened 6 inches and had an angle-of-attack indicator. A total-pressure probe was mounted below the body. Five pulse rockets were located in the cylindrical body section rearward of the wing with exhaust ports along the top of the body.

The model was equipped with a six-channel telemeter incorporating an angle-of-attack indicator, a pressure gage measuring free-stream total pressure, a longitudinal accelerometer, a transverse accelerometer, and two normal accelerometers. The normal accelerometers were located 20.5 inches apart; this arrangement permitted the determination of instantaneous pitching moment in addition to normal force at the model center of gravity.

TESTS

The 75S-T6-solid aluminum-alloy wing of the model was static-tested to determine the deflection response to an arbitrary 30-pound concentrated load applied at points along the wing quarter-chord line.

With instruments installed, the model was suspended by shock cords and vibrated in the pitch plane by an electromagnetic shaker and also by striking the wing and fuselage. The following model natural frequencies and modes of vibration were determined from the telemeter record taken during this ground test and from visual observations of the model vibrating:

Wing, first bending, cps	26 to 27
Wing, second bending, cps	100 to 120
Angle-of-attack boom, cps	84 to 85
Unknown mode, cps	69 to 74
Fuselage rearward of wing, cps	59 to 62

In addition, the natural frequencies of the normal and transverse accelerometers were

Transverse accelerometer, cps	46.6
Forward normal accelerometer, cps	96.5
Rearward normal accelerometer, cps	147.8

The telemeter installation was tested for the effect of shock due to pulse-rocket firing. The model was again suspended by shock cords and static-tested by firing a pulse rocket with the telemeter operating. The telemeter functioned properly. Small-amplitude oscillations with a frequency corresponding to the first bending of the wing were superimposed on the basic oscillations.

An ABL Deacon rocket motor was used to boost the model. This rocket motor delivers approximately 6000 pounds thrust for 3.05 seconds. By contrast, the pulse rockets used to pitch the model develop an average thrust of about 475 pounds for 0.04 second.

The flight time history of the model was recorded by a ground telemeter system which gave six continuous channels of information. A radiosonde released at the time of firing was used to obtain free-stream temperature and static pressure. Additional ground equipment consisting of a CW Doppler radar set and a radar tracking unit was used to determine model velocity and position in space.

The model was flown with the center of gravity located 78.8-percent mean aerodynamic chord ahead of the leading edge of the wing mean aerodynamic chord. The variation with Mach number of Reynolds number and dynamic pressure is presented in figure 4. Also shown in this figure at Mach numbers 0.85, 0.92, 1.3, and 1.4 are the corresponding test conditions for the $\frac{1}{15}$-scale Northrop MX-775A model of reference 2. The range of Reynolds number for the present test was from 3.3×10^6 to 7.6×10^6 based on the wing mean aerodynamic chord of 0.82 foot. Dynamic pressure varied from 650 to 2,460 pounds per square foot.

METHOD OF ANALYSIS

All data reported herein were obtained during the decelerating portion of the flight after separation of the model from the booster.

Trimmed flight.- Since the model in trimmed flight flew at virtually zero normal-force coefficient, the drag coefficient in trimmed flight was assumed equal to the chord-force coefficient. The values of drag coefficient in trimmed flight were calculated by two independent methods. The first method involved the use of a longitudinal accelerometer mounted in the model. The second method involved differentiation with respect to time of the velocity along the flight path as determined by the CW Doppler radar set.

Model pitching.- The lift and drag coefficients were determined by transferring the normal and longitudinal accelerations at the model

center of gravity measured along the body axes to the stability axes. The angle between the two sets of axes was the measured angle of attack corrected to the model center-of-gravity location by the method of reference 3. The normal acceleration at the center of gravity was determined from readings of two normal accelerometers designated a_{n_1} and a_{n_2} which were located 5.30 inches rearward of the center of gravity and 15.15 inches forward of the center of gravity, respectively. The resulting expression for normal acceleration at the model center of gravity was

$$a_{n_{cg}} = 0.741a_{n_1} + 0.259a_{n_2}$$

The instantaneous model pitching acceleration $\ddot{\theta}$ was similarly given by the expression

$$\ddot{\theta} = 0.586\left(a_{n_2} - a_{n_1}\right)$$

The instantaneous pitching moment corrected for the effect of damping was obtained by omitting the last term from the equation

$$C_m = \frac{I_y\ddot{\theta}}{qS\bar{c}} - \dot{\alpha}\left[(C_m)_{\dot{\theta}\bar{c}/2V} + (C_m)_{\dot{\alpha}\bar{c}/2V}\right] - \dot{\gamma}(C_m)_{\dot{\theta}\bar{c}/2V}$$

This correction was necessary since only the sum of the rotational damping coefficients was known; no serious error was introduced since $\dot{\gamma}$ was small compared to $\dot{\alpha}$. The coefficient of lift was plotted against angle of attack, total drag coefficient, and pitching-moment coefficient, all corresponding to one pitching oscillation; and the average Mach number was determined for each oscillation so plotted. The sum of the rotary damping coefficients $(C_m)_{\dot{\theta}\bar{c}/2V} + (C_m)_{\dot{\alpha}\bar{c}/2V}$ was determined from the relationship

$$(C_m)_{\dot{\theta}\bar{c}/2V} + (C_m)_{\dot{\alpha}\bar{c}/2V} = -\frac{8I_y}{\rho VS\bar{c}^2}\left(\frac{0.693}{T_{1/2}} - \frac{C_{L_\alpha}\rho VSg}{4W}\right)$$

Static longitudinal stability was obtained from the instantaneous pitching-moment data and by analyzing the pitching oscillations for the determination of the period and damping of the short-period longitudinal oscillation. Static longitudinal stability was then obtained as follows:

CONFIDENTIAL

$$\frac{\partial C_m}{\partial \alpha} = C_{m_\alpha} = -\frac{I_y}{57.3 q S \bar{c}}\left(\frac{4\pi^2}{p^2} + \frac{0.480}{T_{1/2}^2}\right)$$

$$\frac{\partial C_m}{\partial C_L} = C_{m_{C_L}} = \frac{C_{m_\alpha}}{C_{L_\alpha}}$$

The coefficient C_{L_α} was obtained from a plot of lift coefficient against angle of attack. A third method using the data from the two normal accelerometers directly gave

$$\frac{\partial C_m}{\partial C_L} = \frac{\partial C_m}{\partial C_N} = 0.794 \frac{I_y g}{W \bar{c}}\left(\frac{d\alpha_{n_2}}{d\alpha_{n_{cg}}} - 1\right)$$

The preceding expression is an approximation in that it is uncorrected for the effect of the rotary damping derivatives and was, therefore, used only as a check in connection with the two other methods of obtaining static longitudinal stability.

The periods of the directional oscillations which were induced when the model pitched were analyzed to obtain the derivative of the yawing-moment coefficient due to sideslip C_{n_β}. Values of C_{n_β} were determined from the expression

$$C_{n_\beta} = \frac{4\pi^2 I_z}{P^2 q S b}$$

Aeroelastic correction factors.- The experimental values of model lift-curve slope and aerodynamic-center location were corrected for the effects of aeroelastic distortion of the wing. Correction factors were calculated from static loadings of the wing by the method outlined in the appendix.

ACCURACY

The general limitations of the pulse technique are discussed in reference 4. The accuracy of the data of this test is indicated by figures 5(a) and 6. Figure 5(a) shows close agreement on zero-lift drag between data obtained from Doppler radar and telemeter records. Figure 6 shows typical scatter of the data points obtained from the telemeter when the model pitched. A hysteresis effect is apparent, particularly in the pitching-moment plot of figure 6 as the model pitched up and down. The scatter during model pitching was also increased by the appearance of small-amplitude high-frequency oscillations from 68 to 69 cycles per second which were superimposed on the basic pitching oscillations of the model. Although the telemeter record was faired by enveloping the superimposed oscillations, the accuracy was reduced by their presence. During trimmed flight, these high-frequency oscillations did not occur. The estimated maximum errors in some of the data for the model of the present test in trimmed flight are as follows:

Mach number	±0.010
C_D at Mach number 0.90	±0.001
C_D at Mach number 1.30	±0.0005
C_N at Mach number 0.90	±0.015
C_N at Mach number 1.30	±0.004

For the data obtained over one cycle of an oscillation and related to an average value of Mach number, the estimated maximum variation of Mach number from the average value is ±0.015.

RESULTS

The experimental data from the flight test of the $\frac{1}{10}$-scale Northrop MX-775A stability model are presented in figures 5 to 11.

Trimmed Flight

Figure 5 shows the effect of Mach number on the zero-lift drag and trim normal-force coefficient. The drag curve was largely defined by data obtained from the model in trimmed flight but the curve also includes points obtained when the model pitched through zero lift. The main drag rise occurred approximately at a Mach number of 0.99 and rose from a value of 0.016 at a Mach number of 1.0 to 0.0325 at a Mach number of 1.34. The model was not as clean as the winged model of reference 1 but had slightly lower drag at supersonic Mach numbers due to the more pointed

nose shape. The curve of trim normal-force coefficient shows that the model in trimmed flight was flying very near zero lift. The transonic trim change was very small for the center-of-gravity location tested.

Model Pitching

Lift, drag, and pitching moment.- Basic lift, drag, and pitching-moment data at various Mach numbers are presented in figures 6 and 7. In figure 7 only the faired curves are presented. The approximate range of lift coefficient was 0.3 to -0.2. No corrections for the effect of aeroelastic distortion have been applied to the data presented in these figures. The variations of lift coefficient with angle of attack and pitching-moment coefficient were essentially linear throughout the small range of lift coefficients tested. The variation of lift coefficient with drag coefficient shows that minimum drag occurred near a lift coefficient of 0.1.

Lift and moment-curve slopes.- The effect of Mach number on the coefficients C_{L_α} and C_{m_α} is shown in figure 8. Maximum values occurred at a Mach number of 1. The correction to C_{L_α} for aeroelastic distortion of the 75S-T6 solid-aluminum-alloy wing of the model is seen to be appreciable. The corrected C_{L_α} of the present test is in good agreement with the points obtained from wind-tunnel data of reference 2 at Mach numbers 0.85, 0.92, 1.30, and 1.40 for a $\frac{1}{15}$-scale Northrop MX-775A model. The model of reference 2 had a steel wing and was tested at the lower values of dynamic pressure shown in figure 4(b); therefore, aeroelastic effect on the test data of the reference model is probably very small or negligible. A comparison of the corrected experimental lift-curve slopes of the $\frac{1}{10}$-scale model with the subsonic wing-alone theory of reference 5 and the supersonic wing-alone theory of reference 6 indicates that the subsonic theory predicts lower values of C_{L_α} than were obtained experimentally, whereas the supersonic theory predicts somewhat higher values for the plan form of the test model. The slopes determined from the pitching-moment curves of figure 7(c) and directly from the two normal accelerometers by the methods previously described were in good agreement with pitching-moment slope determined from analysis of the model period and damping.

Longitudinal period and aerodynamic center.- Figure 9 shows the variation with Mach number of the period of the longitudinal oscillation and of the aerodynamic-center location as obtained from analysis of the model period and damping. The period decreased uniformly with increase in Mach number. The aerodynamic-center location corrected for aeroelastic effect moved from the most forward location of 22-percent

mean aerodynamic chord at a Mach number of 0.9 to the most rearward location of 39 percent at $M = 1.34$. The static stability of the configuration increased as the Mach number became supersonic. Comparison with values obtained from the data presented in reference 2 for a $\frac{1}{15}$-scale Northrop MX-775A model indicates an 8 percent more rearward location of aerodynamic center for the $\frac{1}{15}$-scale model. The reason for this difference is not known but may be partly caused by inaccuracy in accounting for the large effect of aeroelasticity on aerodynamic-center location of the $\frac{1}{10}$-scale model of the present test and in transcribing the data of reference 2 to give aerodynamic-center location in percent of mean aerodynamic chord.

Longitudinal damping.- The time required for the pitching oscillations of the model to damp to one-half amplitude is shown in figure 10(a) and the data converted to the rotational damping $(C_m)_{\dot{\theta}\bar{c}/2V} + (C_m)_{\dot{\alpha}\bar{c}/2V}$ are given in figure 10(b). The rotational damping became relatively low at transonic Mach numbers and was at a minimum near $M = 1$. This effect, however, is not too apparent in the total damping of the configuration as shown by figure 10(a). The time to damp to one-half amplitude decreased gradually as the Mach number became supersonic.

Lateral period and C_{n_β}.- The variation with Mach number of the period of the induced lateral oscillations is shown in figure 11(a) by the circled points. For comparison, the longitudinal period indicated by the solid line is also presented. At the lower Mach numbers of the test, the longitudinal period was about one-half that of the lateral period. At these Mach numbers the amplitude of the lateral oscillations was modified by disturbances of approximately the same period as the longitudinal period. The resulting lateral oscillations were somewhat irregular at these low Mach numbers. It is not known whether such irregular effects might occur for the full-scale missile. All lateral oscillations damped toward zero; however, at reduced amplitudes the damping was less, particularly for test Mach numbers greater than 1.

The variation with Mach number of the yawing-moment coefficient due to sideslip C_{n_β} is presented in figure 11(b). The values of C_{n_β} agree well with points at Mach numbers 0.85 and 1.4 obtained from the wind-tunnel data of reference 2 and corrected to the center-of-gravity location of the present test model. The present test values should be lower than the values from reference 2 because of greater flexibility of the magnesium vertical tail of the $\frac{1}{10}$-scale model.

CONCLUSIONS

A flight investigation to determine the longitudinal stability of a $\frac{1}{10}$-scale model of the Northrop MX-775A missile at low lift coefficients through a range of Mach number from 0.89 to 1.34 showed the following results:

1. The lift-curve slope had a maximum value of approximately 0.070 at a Mach number of 1. At this same Mach number the lift-curve slope corrected for the effect of aeroelastic distortion was 0.095.

2. The aerodynamic center moved from the most forward location of 10-percent mean aerodynamic chord at a Mach number of 0.9 to the most rearward location of 20-percent mean aerodynamic chord at $M = 1.2$. The aerodynamic center corrected for aeroelastic effect moved from 22-percent mean aerodynamic chord at a Mach number of 0.9 to the most rearward location of 39 percent at $M = 1.34$. The static stability increased as the Mach number became supersonic.

3. The rotational damping $(C_m)_{\dot{\theta}\bar{c}/2V} + (C_m)_{\dot{\alpha}\bar{c}/2V}$ became relatively low at transonic Mach numbers and was at a minimum near $M = 1$; however, the total damping increased as the Mach number became supersonic.

Langley Aeronautical Laboratory,
National Advisory Committee for Aeronautics,
Langley Field, Va.

Warren Gillespie, Jr.
Warren Gillespie, Jr.
Aeronautical Research Scientist

Richard G. Arbic
Richard G. Arbic
Aeronautical Research Scientist

Approved:

P R Hill
for Joseph A. Shortal
Chief of Pilotless Aircraft Research Division

cig

APPENDIX

AEROELASTIC CORRECTION FACTORS

The correction factors for the effects of aeroelastic distortion were determined from static loadings of the wing in conjunction with a modified strip theory. The incremental lift change due to elasticity was considered to be a function of the incremental local angle-of-attack change due to elasticity. The loading at any spanwise station was then given by the product of the ratio of the local angle of attack to the angle of attack of the root section and the expression for the rigid wing loading at any spanwise station. The method of reference 5 was used to obtain the spanwise load distribution for the rigid wing. This distribution was assumed to hold throughout the Mach number range of the test. By using the data of figure 12, the total measured flight load was distributed over the wing in such a manner that the additional loading due to aeroelastic deflection when added to the applied loading gave the spanwise distribution of the rigid wing. Figure 13(a) shows the rigid wing distribution and the distributions determined for the measured lift at Mach numbers of 0.9, 1.1, and 1.3. Figure 13(b) shows the calculated wing twist that would result from the application of the measured lift distributed in the manner shown above. Figure 13(c) shows the corresponding incremental lift distribution determined by the modified strip theory. The incremental lift $\Delta L/\alpha$ corresponding to the change in angle of attack was calculated by the equation

$$\frac{\Delta L}{\alpha} = 2C_{L_\alpha} c_{ave} q \int_0^{b/2} \frac{\Delta\alpha}{\alpha} \frac{(C_l c)}{C_L c_{ave}} dy$$

The correction factor K (fig. 14(a)) was determined by the relation $K = \frac{(L + \Delta L)}{L}$ where L is the measured lift.

The correction factor $\Delta\left(\frac{\partial C_m}{\partial C_L}\right)$ that was used to account for the change in aerodynamic-center position due to aeroelastic distortion was calculated by the equation

$$\Delta\left(\frac{\partial C_m}{\partial C_L}\right) = \left(\frac{\bar{y} - \bar{y}_{\Delta L}}{\bar{c}} \tan \Lambda_{c/4}\right)(K - 1)$$

This correction is based on the inboard movement of the lateral center of pressure that results from the reduction in lift due to aeroelastic wing twist. The correction to the aerodynamic-center location is plotted in figure 14(b).

The previous corrections have neglected the effect of wing-inertia loading acting in opposition to the aerodynamic loading. The inertia loading would be roughly proportional to the ratio of the wing weight and the model weight. Since this ratio is small, additional calculations of the aeroelastic inertia loading effect were not made.

REFERENCES

1. Gillespie, Warren, Jr., and Arbic, Richard G.: Large-Scale Flight Measurements of Zero-Lift Drag at Mach Numbers From 0.87 to 1.39 of $\frac{1}{10}$-Scale Models of the Northrop MX-775A Missile. NACA RM SL51K07, U. S. Air Force, 1951.

2. Phelps, E. Ray, and Lazzeroni, Frank A.: Wind-Tunnel Investigation of the Aerodynamic Characteristics of a $\frac{1}{15}$-Scale Model of the Northrop MX-775A Missile. NACA RM A51E28, 1951.

3. Mitchell, Jesse L., and Peck, Robert F.: An NACA Vane-Type Angle-of-Attack Indicator for Use at Subsonic and Supersonic Speeds. NACA RM L9F28a, 1949.

4. Gillis, Clarence L., Peck, Robert F., and Vitale, A. James: Preliminary Results From a Free-Flight Investigation at Transonic and Supersonic Speeds of the Longitudinal Stability and Control Characteristics of an Airplane Configuration With a Thin Straight Wing of Aspect Ratio 3. NACA RM L9K25a, 1950.

5. DeYoung, John, and Harper, Charles W.: Theoretical Symmetric Span Loading at Subsonic Speeds for Wings Having Arbitrary Plan Form. NACA Rep. 921, 1948.

6. Malvestuto, Frank S., Jr., Margolis, Kenneth, and Ribner, Herbert S.: Theoretical Lift and Damping in Roll at Supersonic Speeds of Thin Sweptback Tapered Wings With Streamwise Tips, Subsonic Leading Edges, and Supersonic Trailing Edges. NACA Rep. 970, 1950. (Supersedes NACA TN 1860.)

TABLE I

PHYSICAL CHARACTERISTICS OF A $\frac{1}{10}$-SCALE MODEL OF THE NORTHROP MX-775A MISSILE

Wing:	
Area (included), sq ft	3.27
Span, ft	4.23
Aspect ratio	5.5
Mean aerodynamic chord, ft	0.82
Sweepback of 0.4 chord, deg	45
Dihedral (relative to mean thickness line), deg	0
Taper ratio, Tip chord/Root chord	0.4
Vertical tail:	
Area (extended to center line), sq ft	0.45
Height (above fuselage center line), ft	1
Sweepback of 0.4 chord, deg	33
Taper ratio, Tip chord/Root chord	0.286
Weight and balance:	
Weight, lb	88.7
Wing loading, lb/sq ft	27.1
Center-of-gravity position (percent $\bar{c}$ forward of leading edge)	78.8
Moment of inertia in pitch, I_y, slug-ft^2	8.90
Moment of inertia in yaw, I_z, slug-ft^2	8.90

TABLE II

BODY, WING, AND VERTICAL-TAIL ORDINATES

Body ordinates		Wing ordinates			Vertical-tail ordinates	
Station, in. from nose	Radius, in.	Percent chord			Percent chord	
		Station	Upper	Lower	Station	Upper and lower
0	0	0	-0.850	0.850	0	0
1.4	.380	1.25	.200	1.573	1.25	.960
2.0	.548	2.50	.610	1.855	2.50	1.335
4.0	1.066	5.00	1.120	2.190	5.00	1.770
6.0	1.502	7.50	1.480	2.410	7.50	2.060
8.0	1.857	10.00	1.773	2.567	10.00	2.265
10.0	2.151	15.00	2.227	2.782	15.00	2.567
12.0	2.390	20.00	2.532	2.922	20.00	2.770
14.0	2.575	25.00	2.747	2.998	25.00	2.907
17.0	2.770	30.00	2.900	3.033	30.00	3.010
20.0	2.878	35.00	2.980	3.040	40.00	3.120
22.0	2.900	40.00	3.010	3.020	50.00	3.057
Straight line		50.00	2.855	2.860	60.00	2.810
65.0	2.900	60.00	2.380	2.380	70.00	2.395
68.0	2.875	70.00	1.812	1.812	75.00	2.090
70.0	2.810	80.00	1.233	1.233	Straight line	
72.0	2.700	90.00	.640	.640	100.00	.100
74.0	2.545	100.00	.015	.015		
76.0	2.340					
78.0	2.070					
80.0	1.710					
80.9	1.500					

NACA

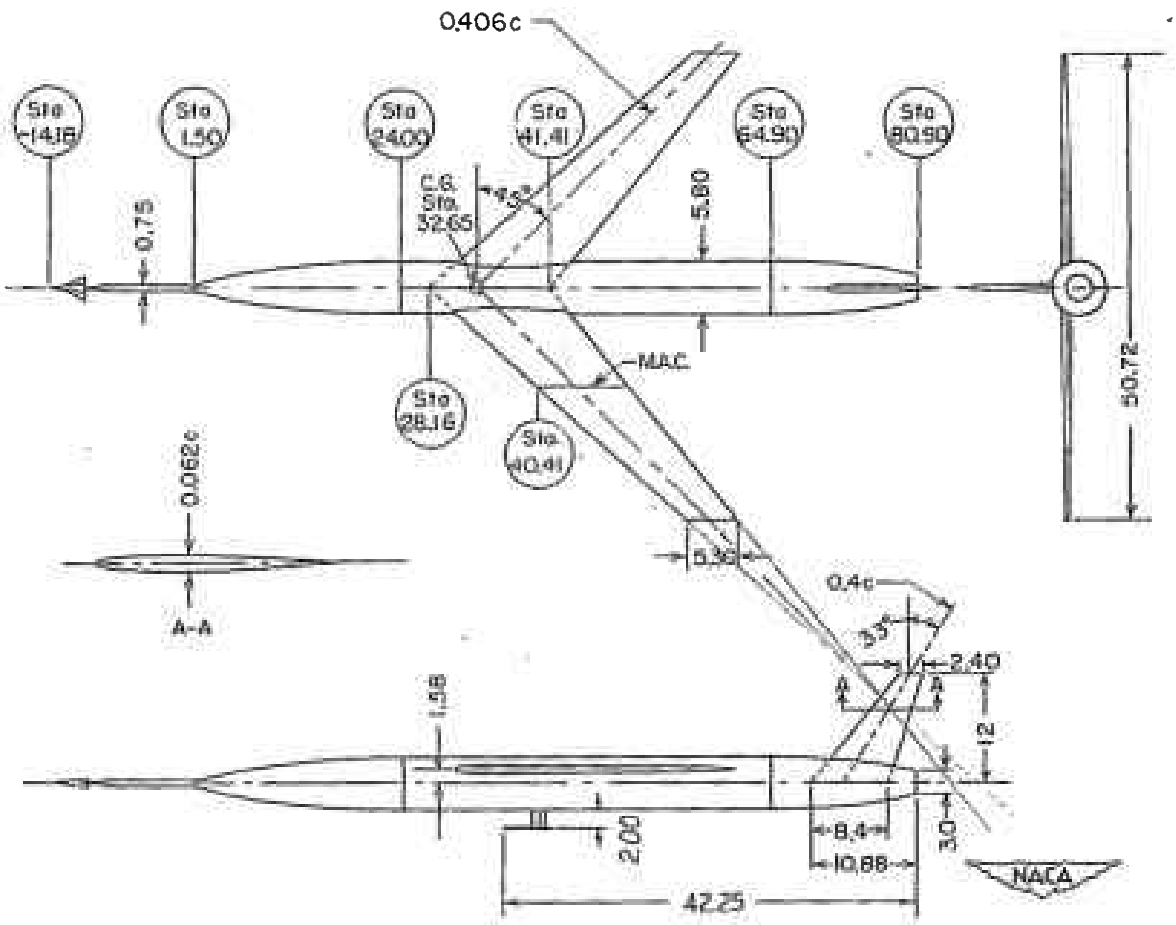

Figure 1.- General arrangement of test model. All dimensions are in inches.

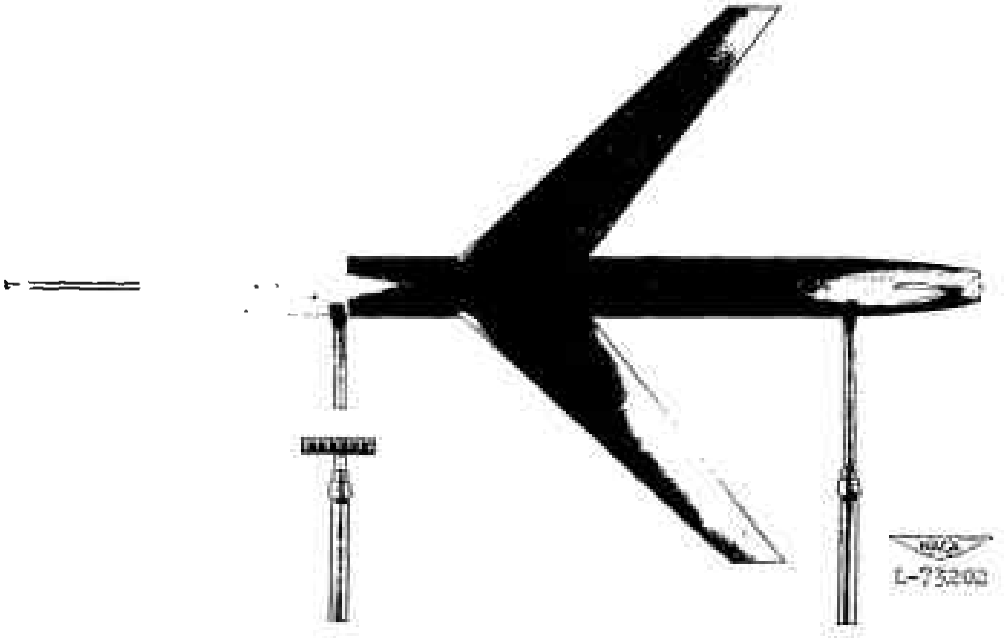

(a) Top view.

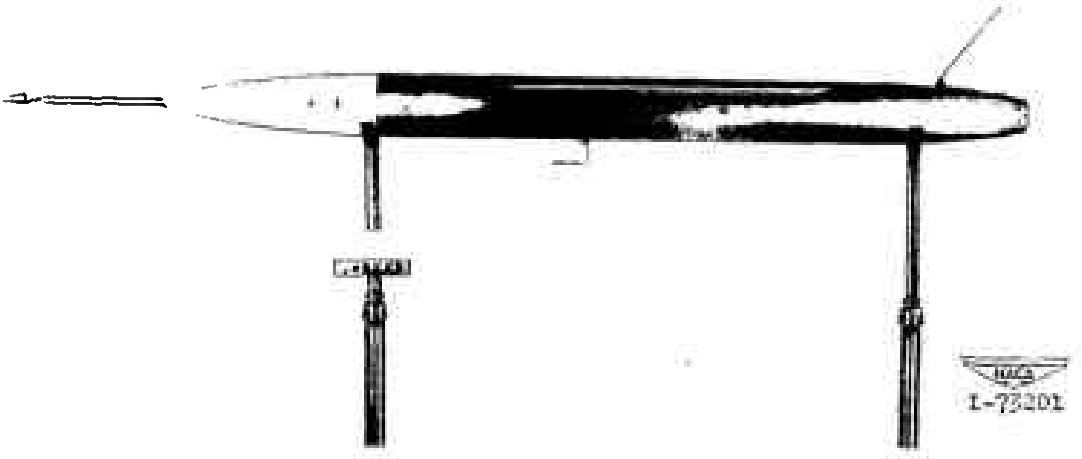

(b) Side view.

Figure 2.- Photographs of 1/10-scale model of Northrop MX-775A missile.

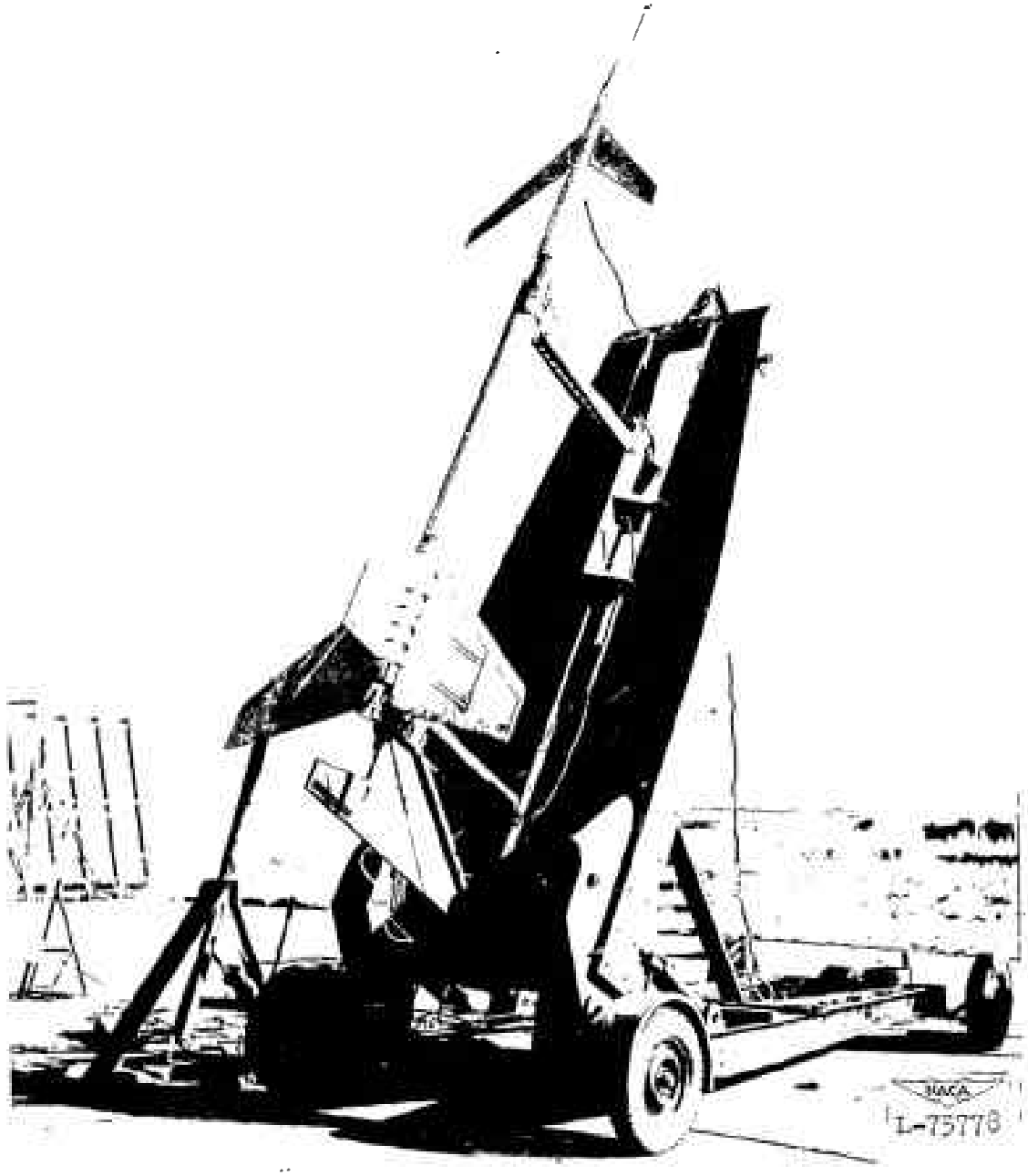

Figure 3.- Model-booster combination in launching attitude.

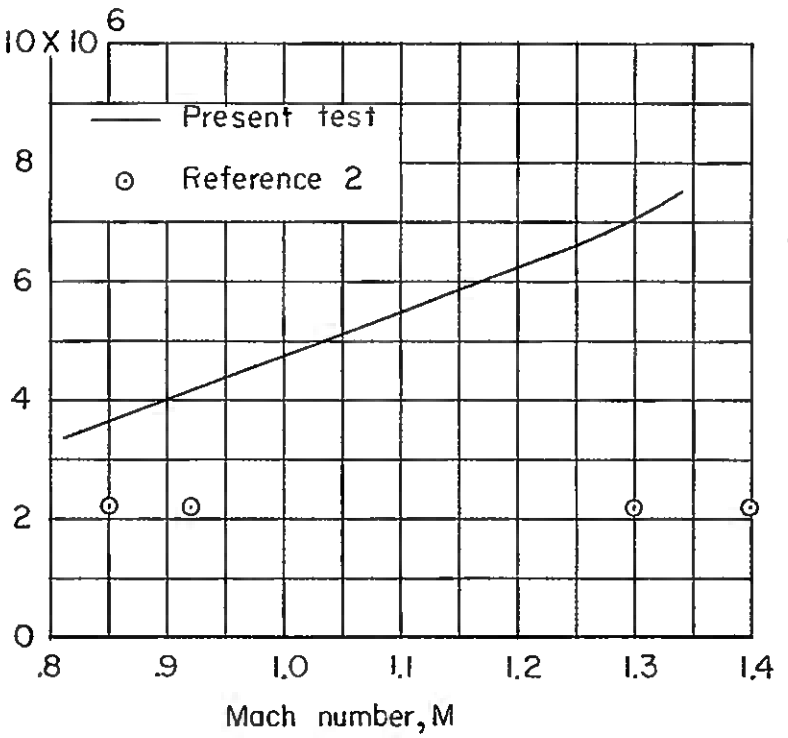

(a) Reynolds number.

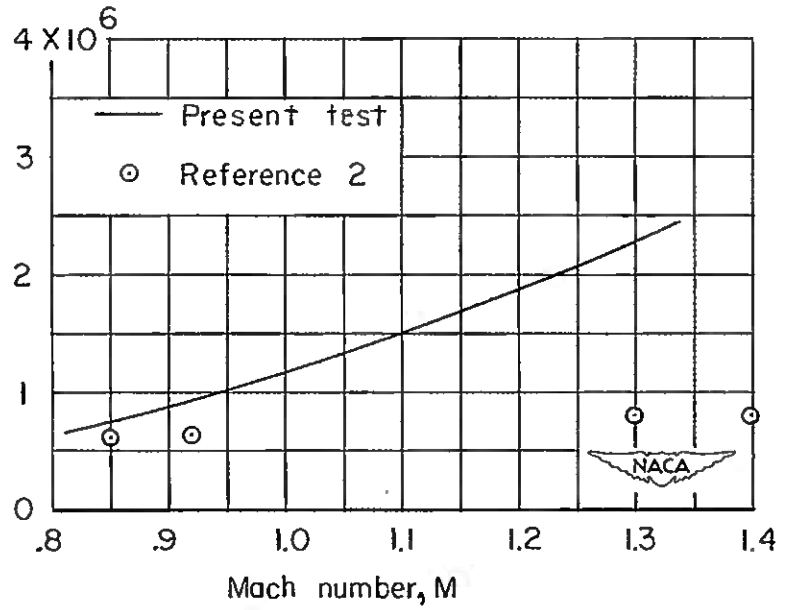

(b) Dynamic pressure.

Figure 4.- Variation of Reynolds number and dynamic pressure with Mach number.

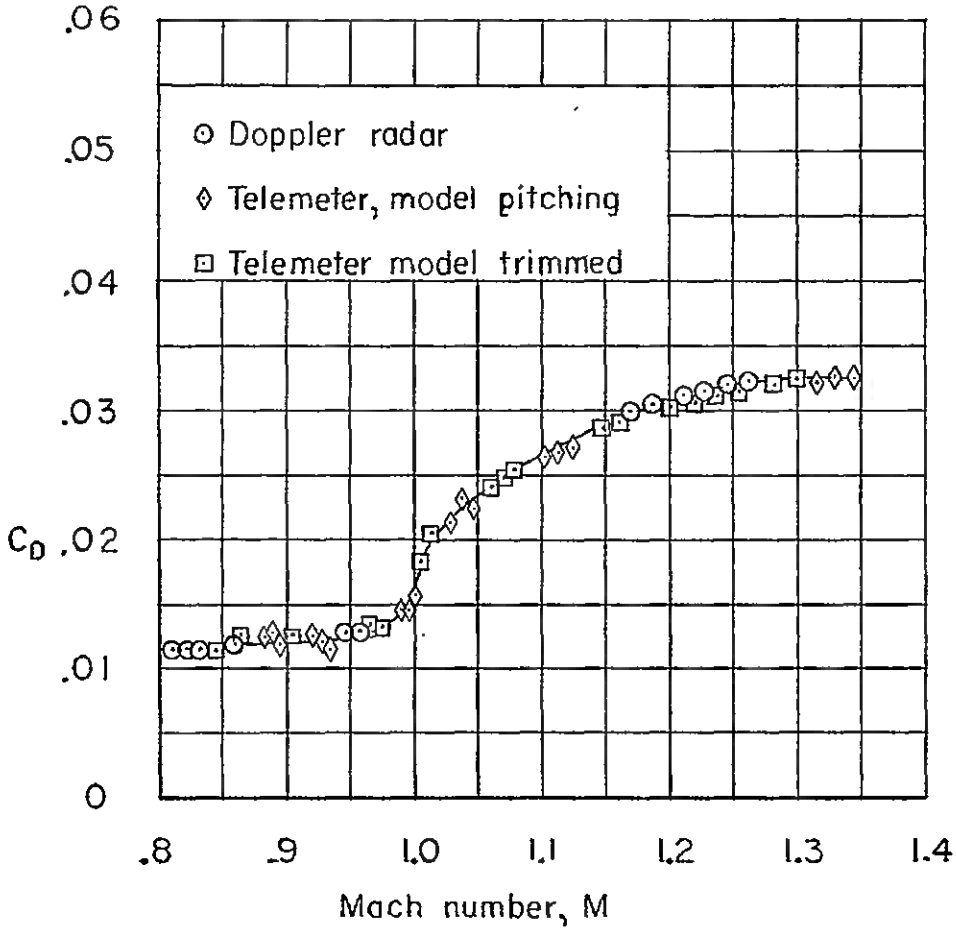

(a) Zero-lift drag.

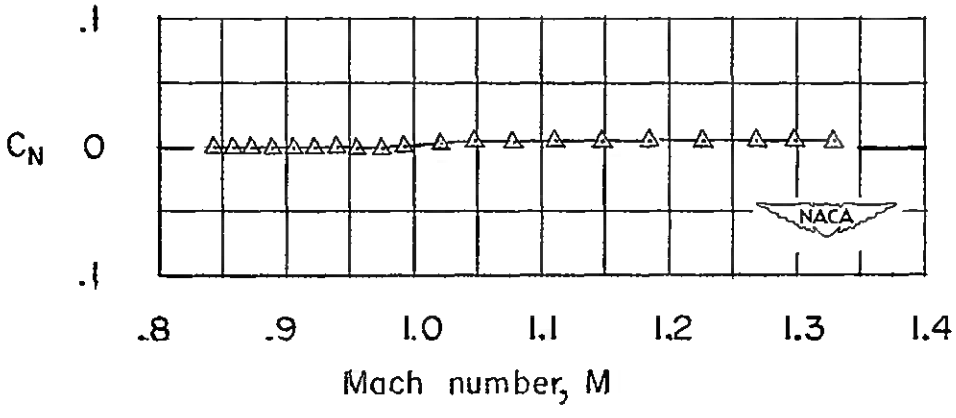

(b) Trim normal-force coefficient.

Figure 5.- Effect of Mach number on the zero-lift drag and trim normal-force coefficient.

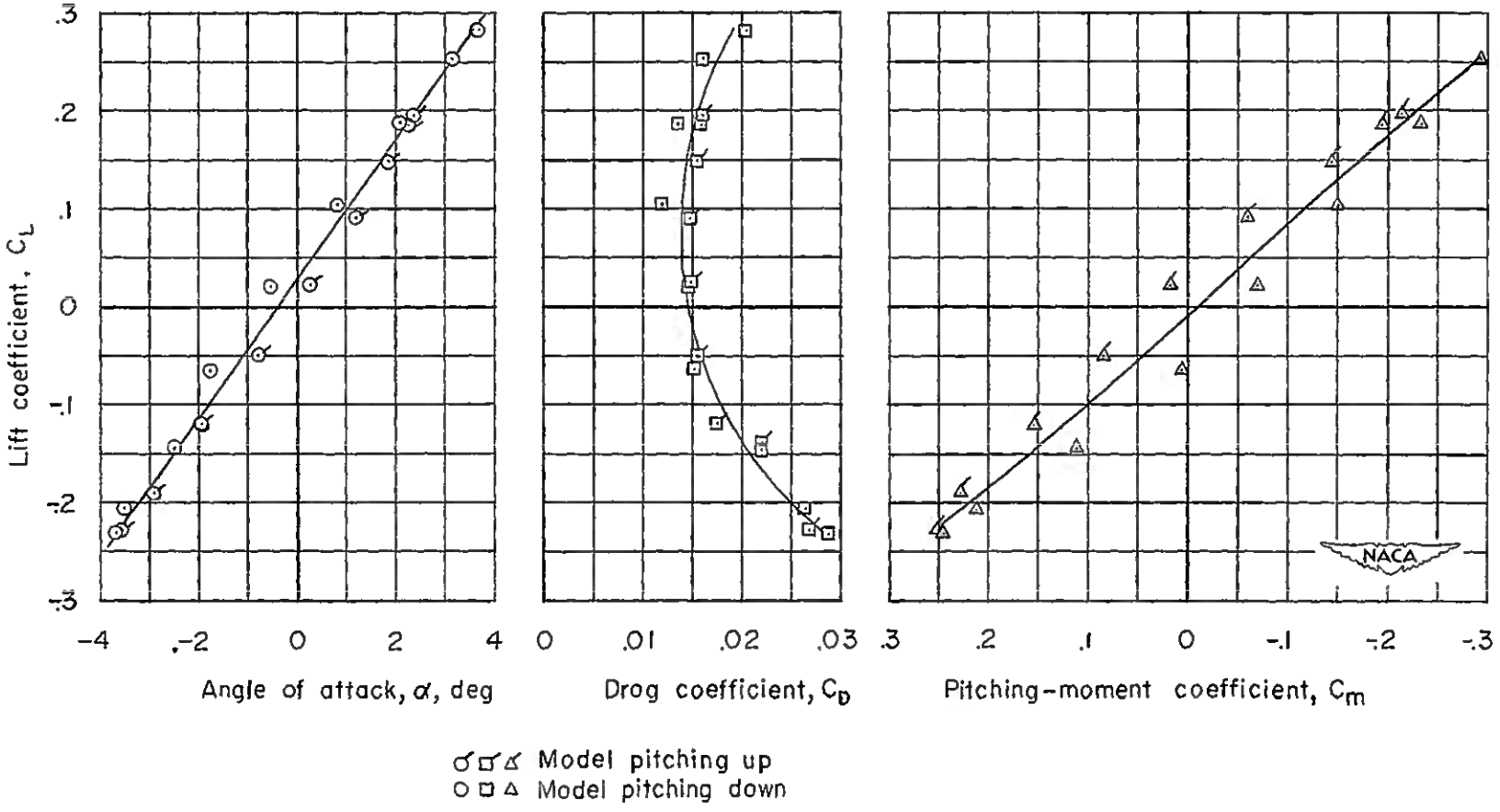

Figure 6.- Variation with lift coefficient of angle of attack, drag coefficient, and pitching-moment coefficient at $M = 0.996$ showing typical scatter of basic data points.

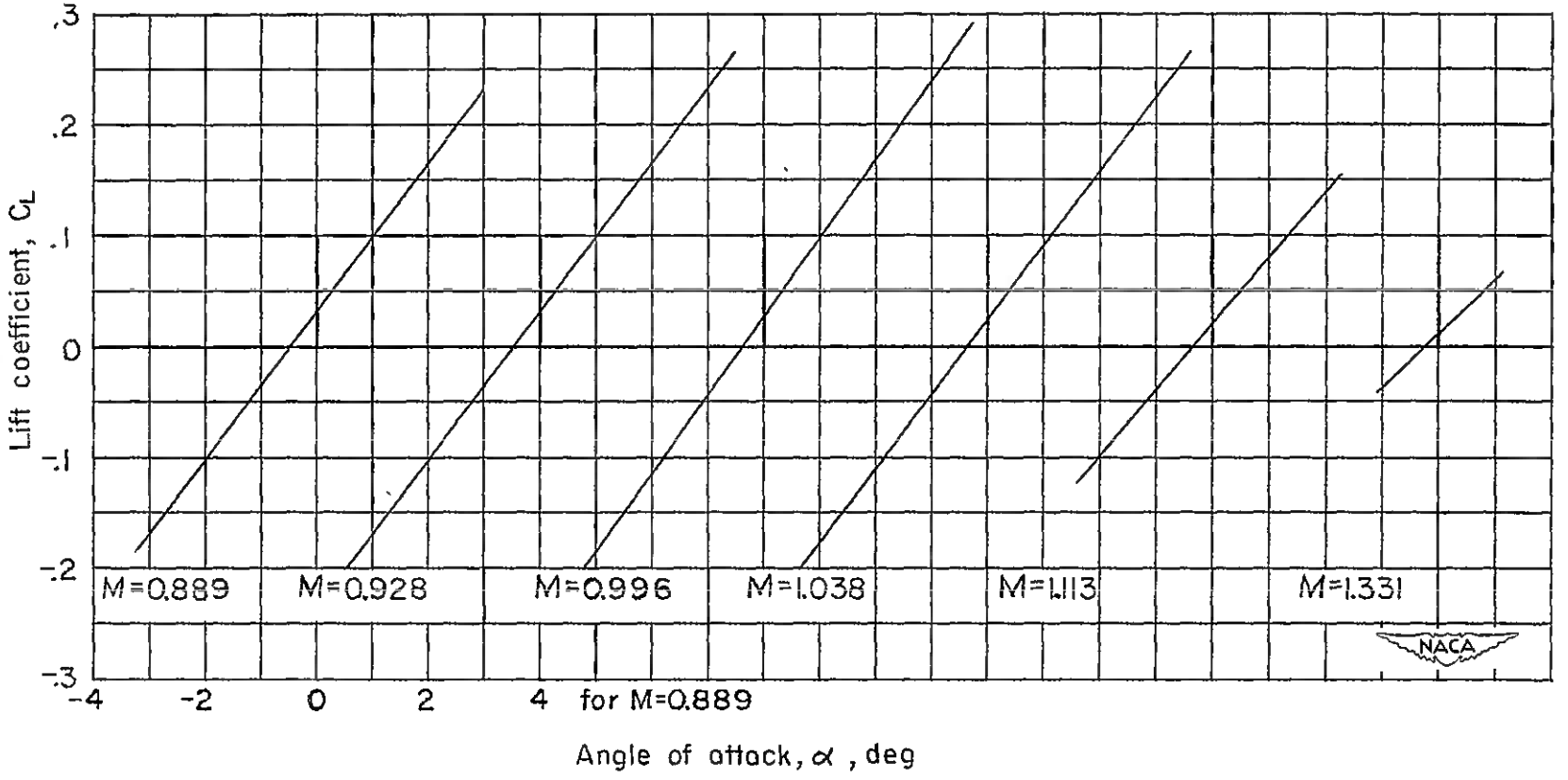

(a) Lift.

Figure 7.- Lift, drag, and pitching moment at various Mach numbers. Note the use of staggered axes.

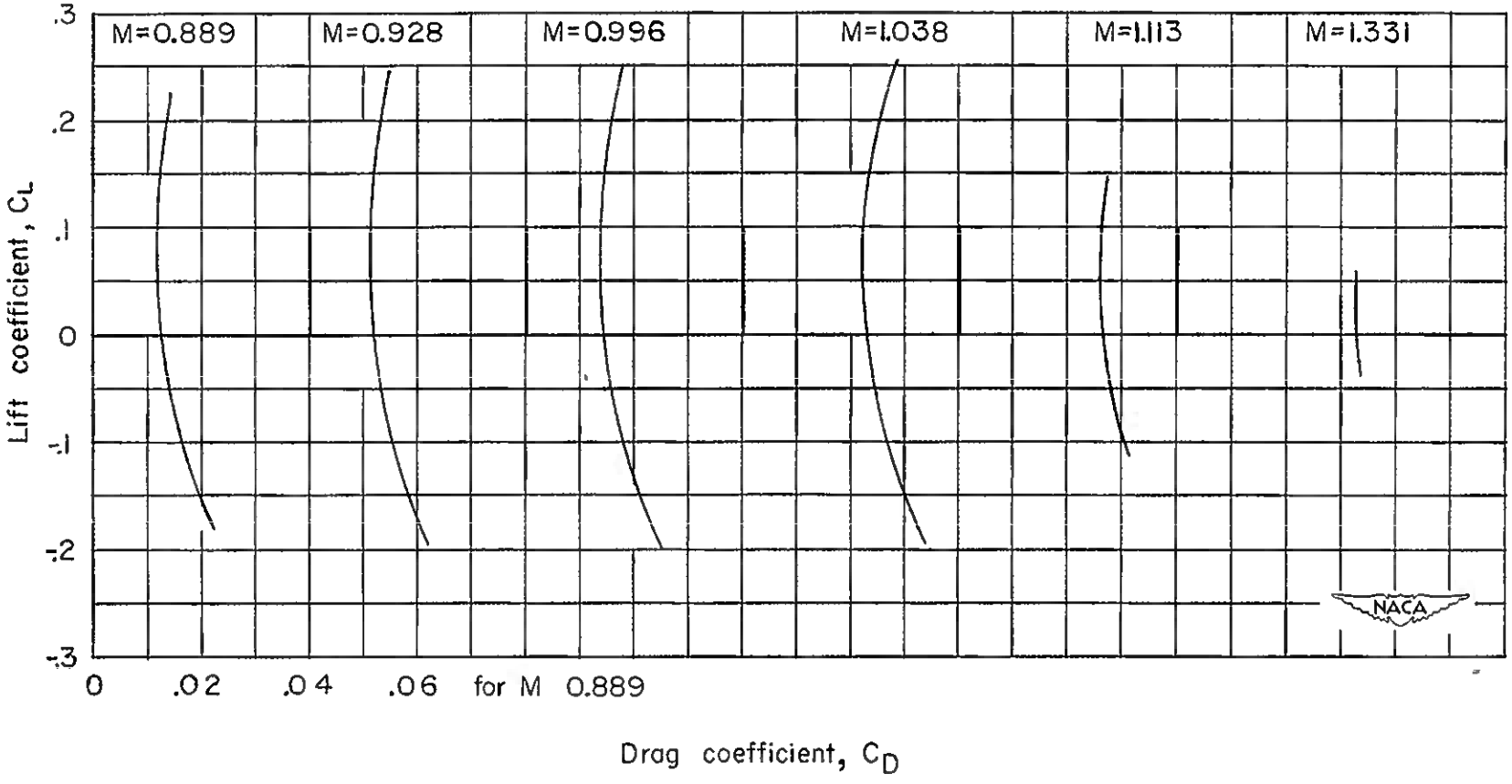

(b) Drag.

Figure 7.- Continued.

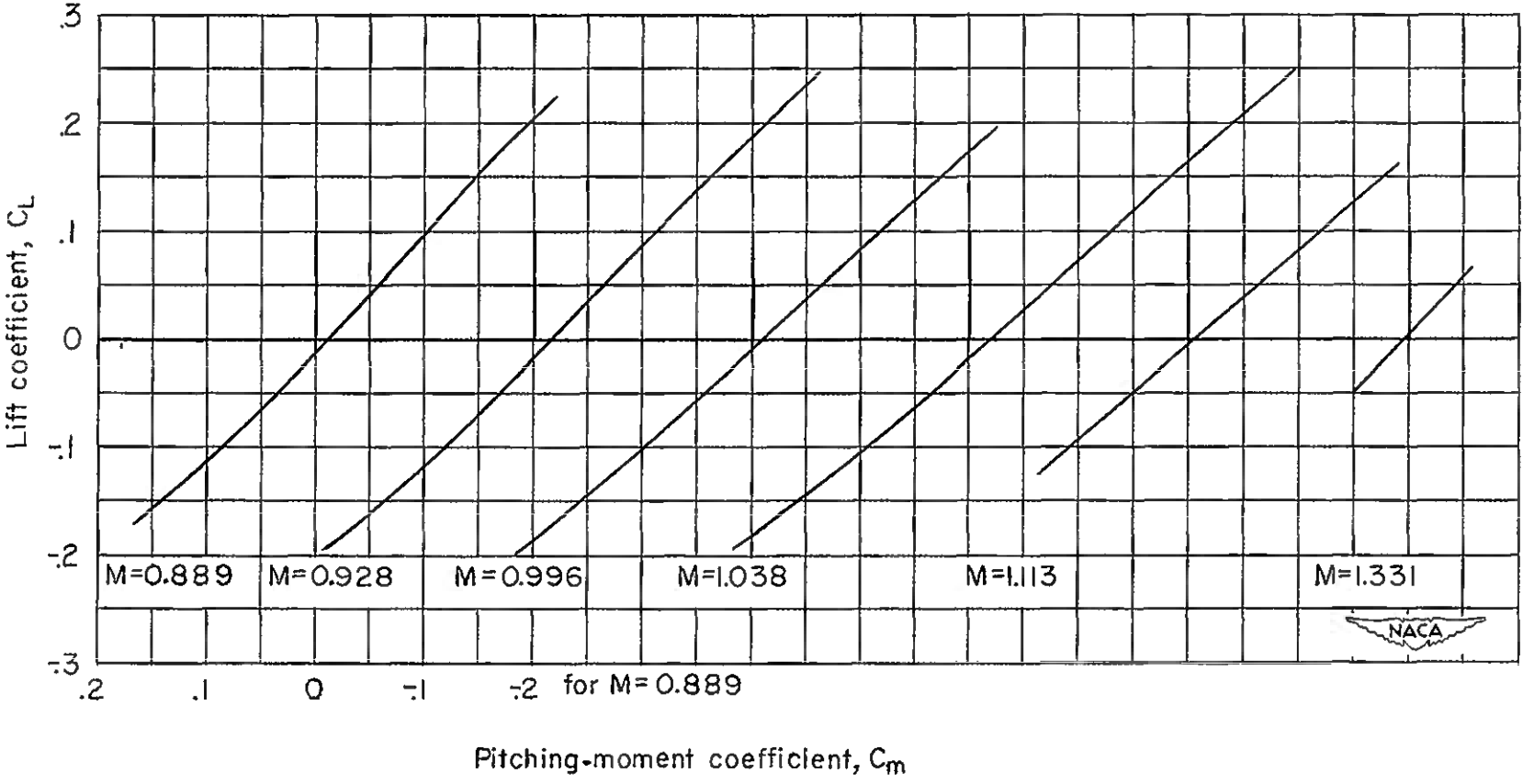

(c) Pitching moment.

Figure 7.- Concluded.

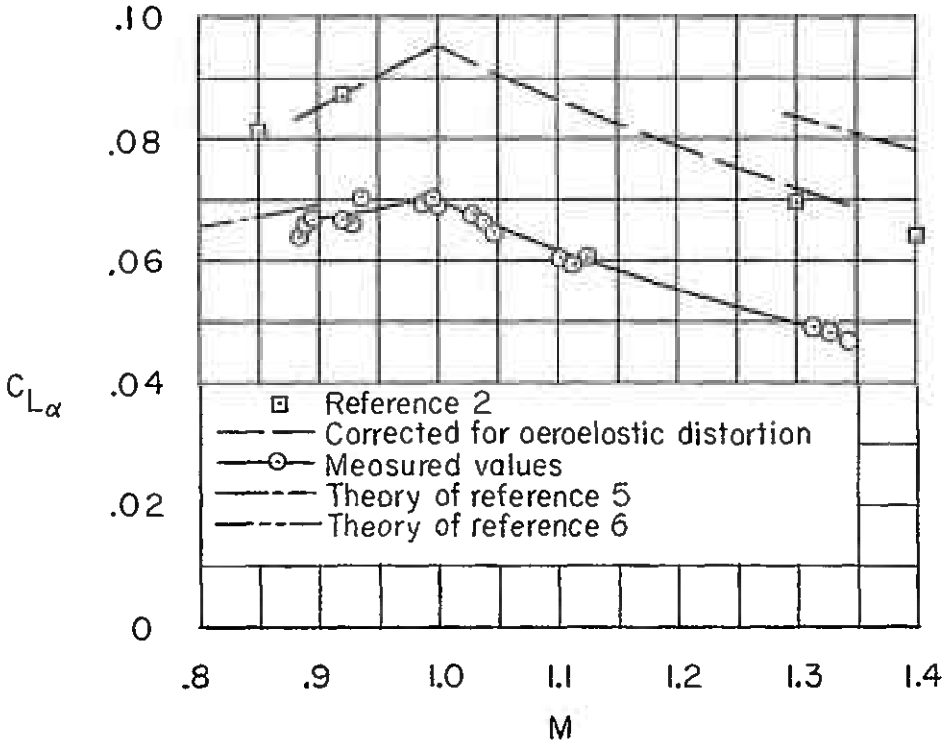

(a) Lift-curve slope.

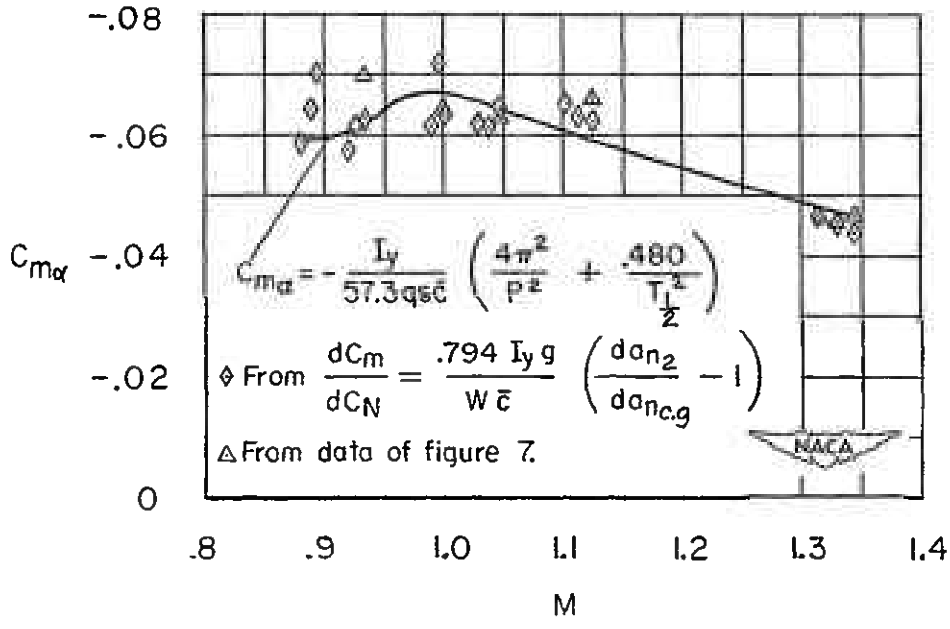

(b) Pitching-moment slope.

Figure 8.- Effect of Mach number on the lift-curve and pitching-moment slopes.

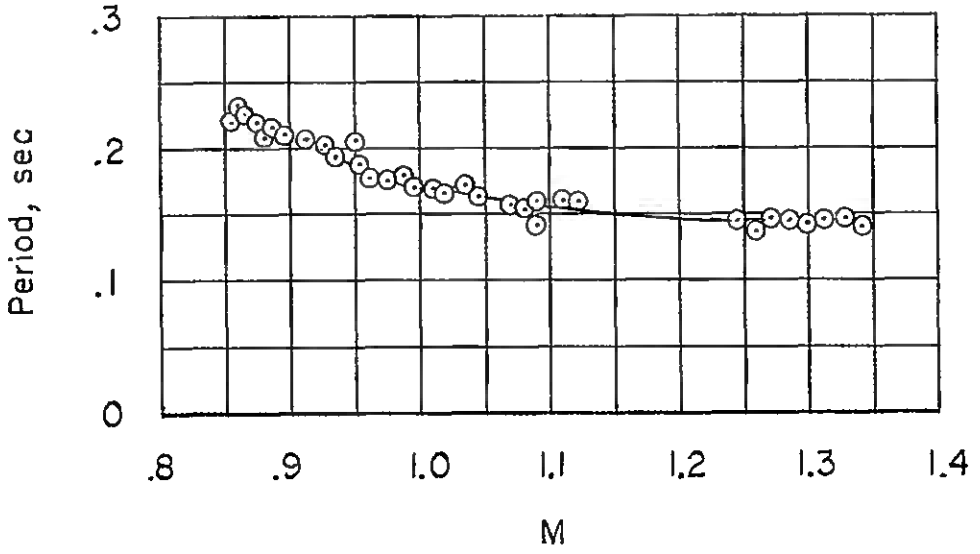

(a) Period of the longitudinal oscillation.

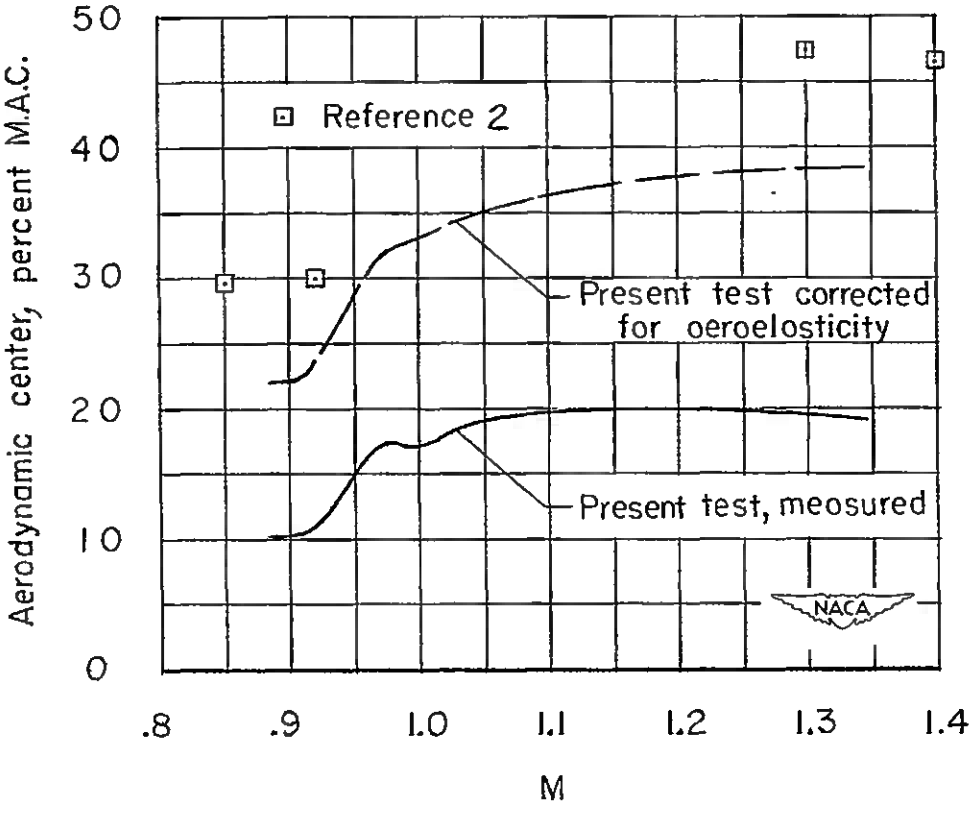

(b) Aerodynamic-center location.

Figure 9.- Variation with Mach number of the period of the longitudinal oscillation and of the aerodynamic-center location.

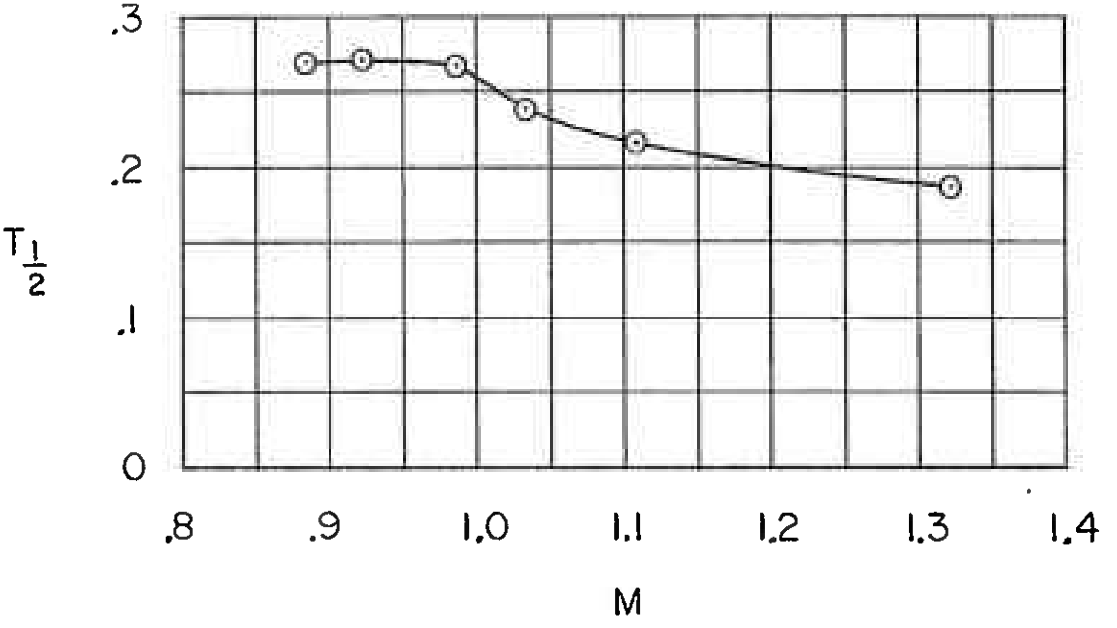

(a) Time to damp to one-half amplitude.

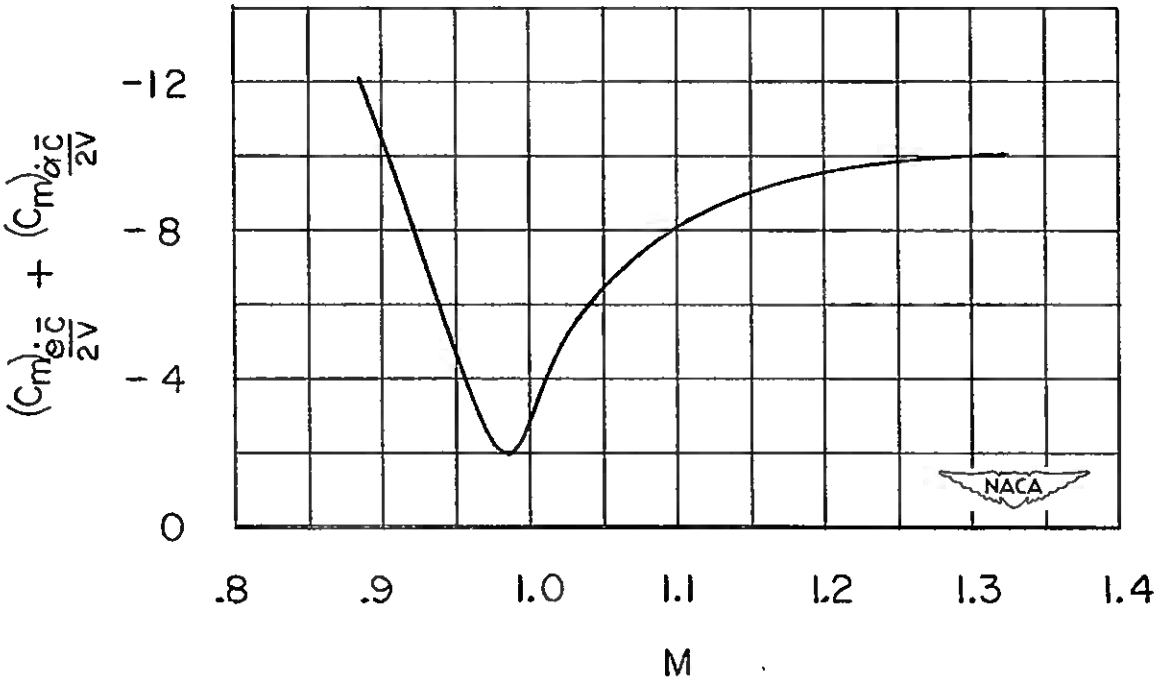

(b) Damping derivatives.

Figure 10.- Damping characteristics of the short-period oscillation.

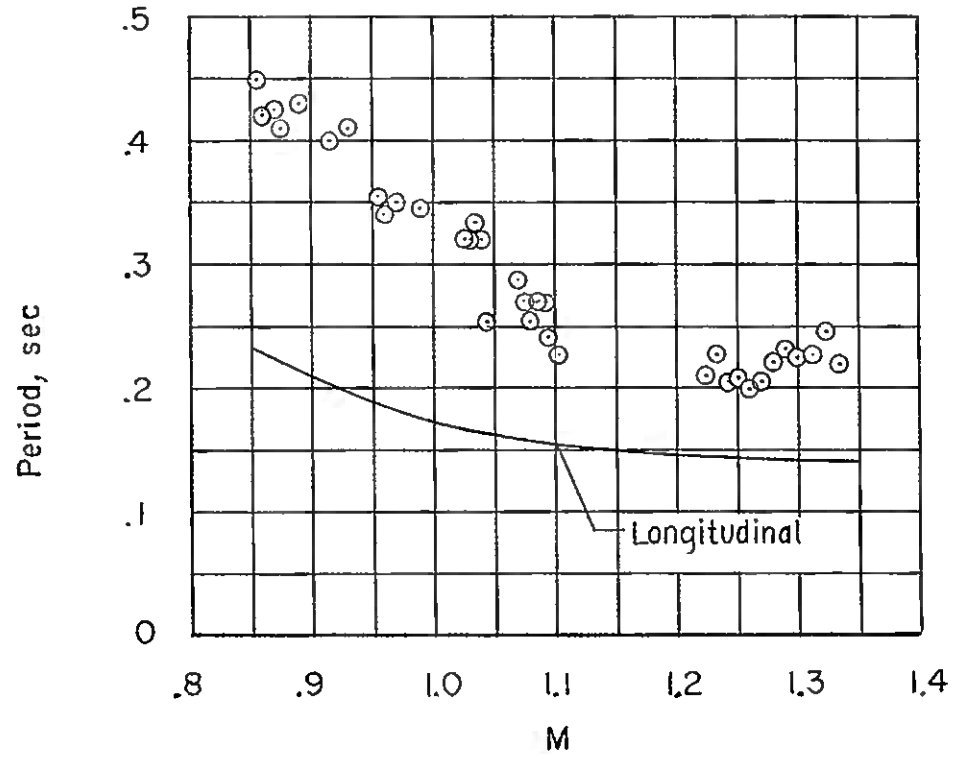

(a) Period of the lateral oscillation.

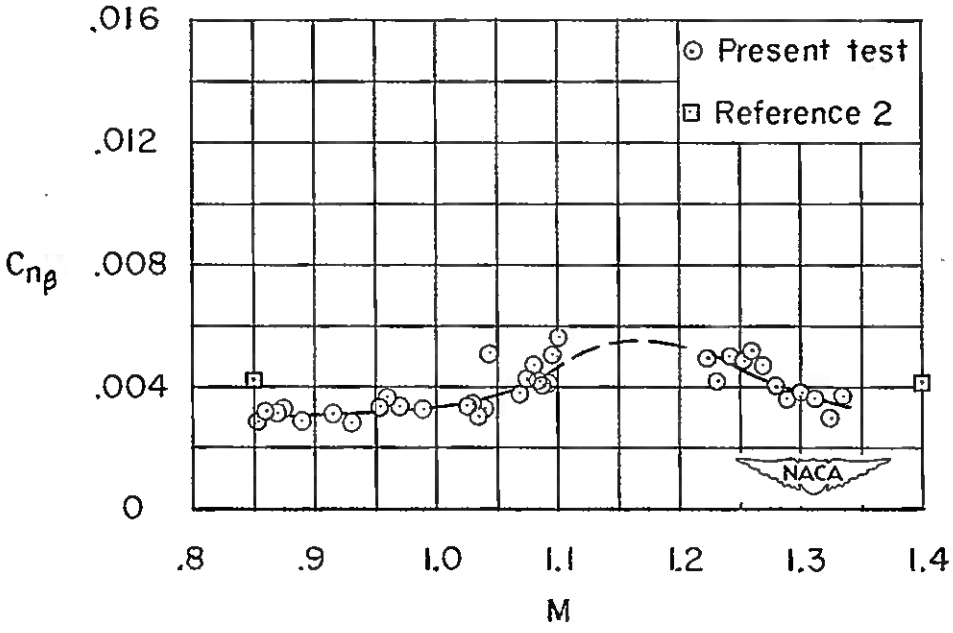

(b) Yawing-moment slope.

Figure 11.- Characteristics of the lateral oscillation.

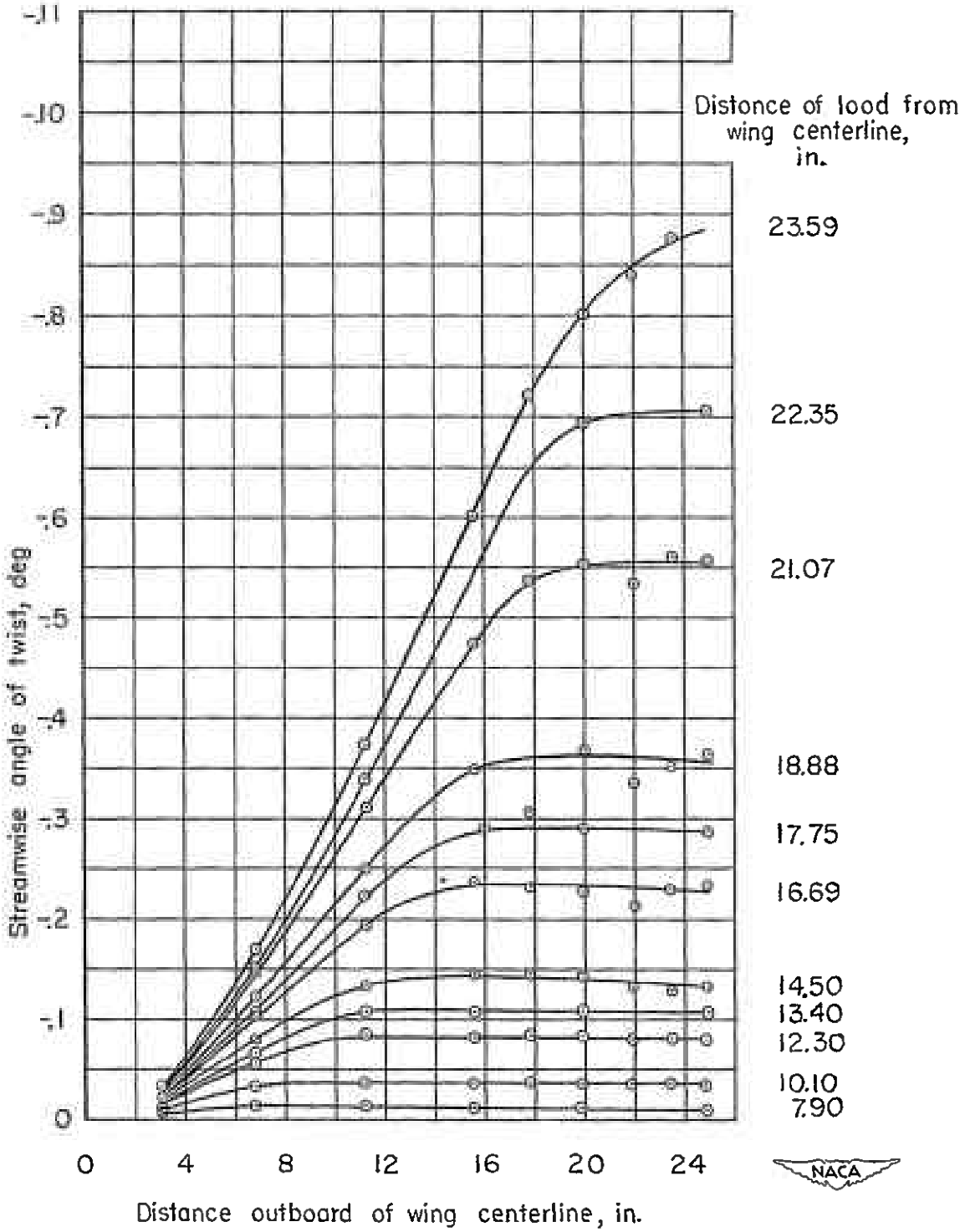

Figure 12.- Streamwise angle of twist of the model wing due to a 30-pound load applied along the 25-percent streamwise chord line and at the spanwise stations indicated.

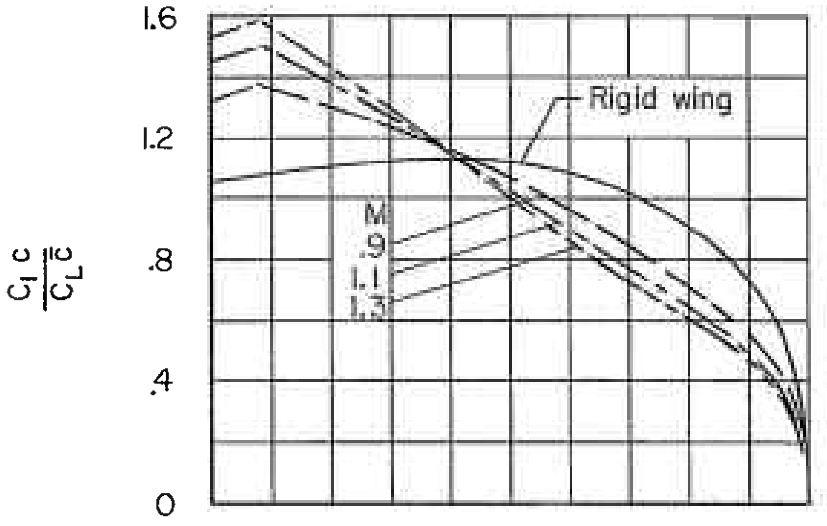

(a) Spanwise load distribution at equal lift coefficients.

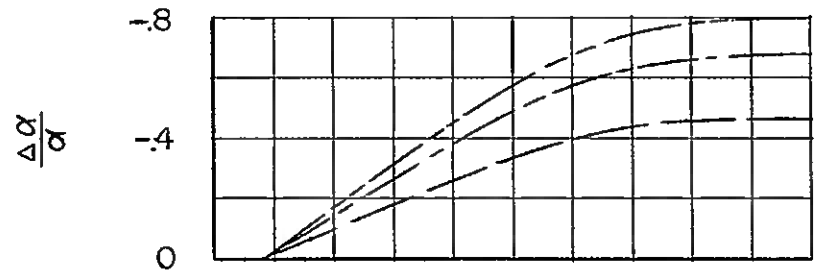

(b) Wing twist.

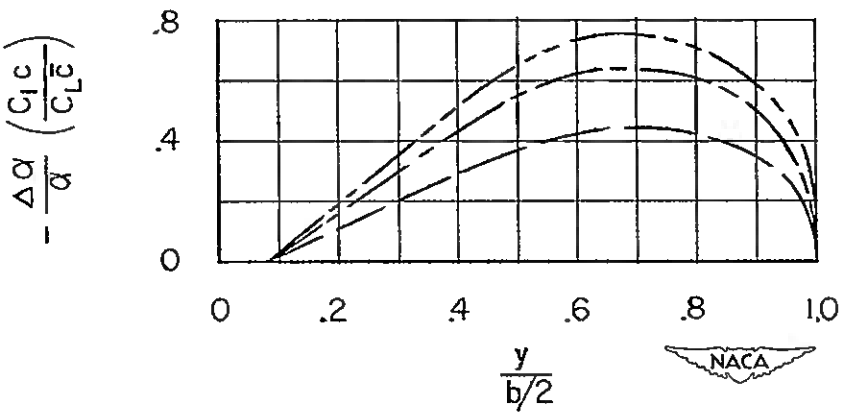

(c) Loss in lift.

Figure 13.- Calculated effect of aeroelasticity on the spanwise load distribution, wing twist, and decremental lift.

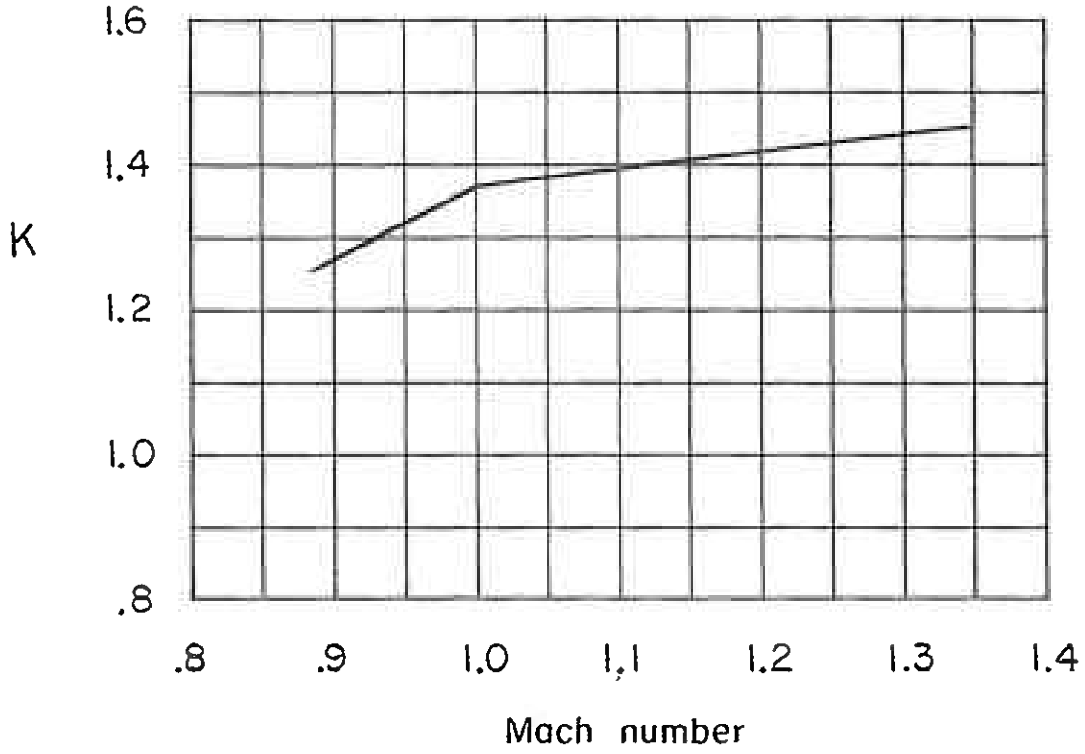

(a) Correction to the lift-curve slope.

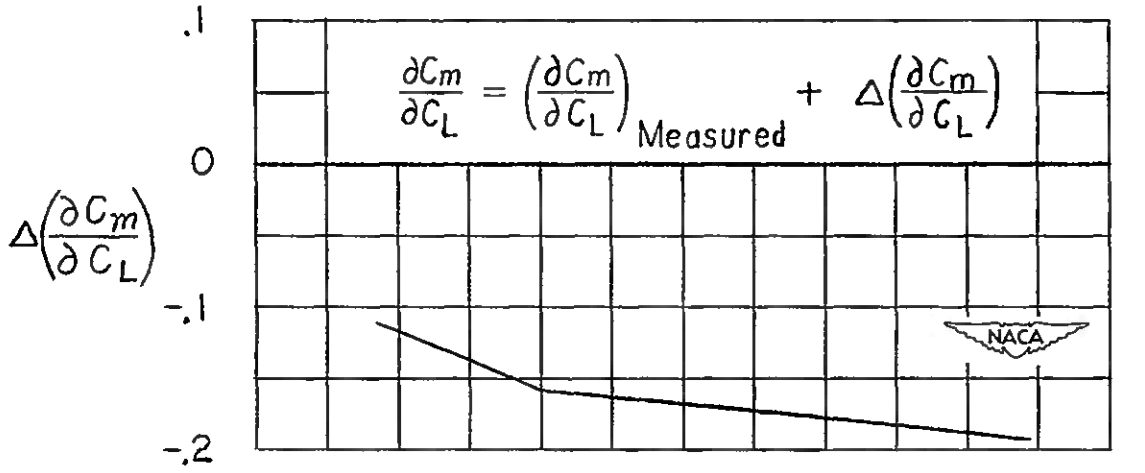

(b) Correction to the aerodynamic-center location.

Figure 14.- Correction factors used to correct the experimental data for the effects of aeroelastic distortion.

[redacted]

SECURITY INFORMATION

[redacted]